Nanoscale patterns in carbon–nickel nanocomposite thin films investigated by AFM and stereometric analysis

Ştefan Ţălu, Katarzyna Janus, and Sebastian Stach

Abstract—The objective of this study is a stereometric investigation of 3-D surface topography of the nickel–carbon (Ni–C) nanocomposite thin films composed of Ni nanoparticles with different average sizes embedded in amorphous hydrogenated carbon, prepared by RF-PECVD. The deposition time was varied at 7, 10 and 13 min, respectively, to study changes in the properties of the obtained films. The studied samples were taken with the help of atomic force microscopy (AFM) operating in a non-contact mode and examined in order to determine their stereometric surface engineering characteristics. This analysis of 3-D surface texture will give a deeper insight into their texture characteristics and their implementation in graphical models and computer simulation.

Keywords— Nickel–Carbon (Ni–C) nanocomposite thin films, stereometric analysis, three-dimensional surface micromorphology.

I. INTRODUCTION

TODAY, due to the broad applications that materials and components have found in the field of nanotechnology, many studies have led on topics such as optimizing the properties of nanostructures, accurate understanding of the growth mechanism of thin films, as well as finding their new applications indicating their extent application in various industrial and medical fields [1]-[7]. Hence, it is very important to use a method to produce the exact favorable nanostructure through a no-bake step [8]-[11].

The properties of thin films mainly depend on chemical composition, crystal structure and their morphology, so multilayer structures of magnetic and non-magnetic metals in the nanometer scale have been attracted attention due to their desirable mechanical and magnetic properties [12]-[22].

Thus, owing to unique properties close to natural diamond, using the Diamond-like carbon (DLC) nanolayer has found many applications; high mechanical stiffness, optical transparency, corrosion resistance and using this layer as a protective coating is widely used in the medical and automotive industries [23]-[33].

One of the important characteristics of DLC is the high electrical resistance these layers. In some electrical applications, layers with higher electrical conductivity are required. To overcome the limitations of these layers including decrease the inner tensions and increase adhesion of films to the substrate, the carbon-metal layers have been produced so that have better properties than DLC.

Therefore, using nickel as carbon composite can have a variety of applications in the fields of optical coatings, catalyst, and water splitting electrode [34]-[38] because this metal has the fcc structure with low lattice mismatch and also due to a variety of alloys and applications can have interesting physical properties along with carbon [39]-[40].

In this study, to determine the thin films surface morphology, the field parameters of nanoparticles of nickel-carbon layers prepared by RF-PECVD are studied using atomic force microscopy (AFM).

II. MATERIALS AND METHODS

A. Samples Preparation

Ni–C composite thin films were prepared by the methodology described elsewhere [2]. Nickel thin films in carbon bed are produced using RF-PECVD instrument that is a combination of two methods of the sputtering and the chemical vapor deposition. In this sputtering method, ions and gas react with the target and the produced layers are composed of the sputtered target material and the reactive gas.

In this device, two rotary and diffusion pumps are used to vacuum the steel chamber. The chamber consists of two electrodes with a radius of 7.5 cm (target electrode) and a radius of 13 cm (substrate) so that the smaller electrode is connected to the RF source and the other one is connected to the ground via the chamber. The source frequency is 13.56 MHz that is applied to the electrodes as capacitor, and the distance between the electrodes is 5 cm.

The used substrates, glass and silicon, are 1×1 dimension so that they are washed with water and soap too clean up the pollution and then they are placed in acetone for 5 minutes in

Ştefan Ţălu is with The Technical University of Cluj-Napoca, The Directorate of Research, Development and Innovation Management (DMCDI), Constantin Daicoviciu Street, no. 15, Cluj-Napoca, 400020, Cluj county, Romania, http://research.utcluj.ro (corresponding author, phone: +0040-264–401200; fax: +0040-264–592055; e-mail: stefan_ta@yahoo.com).

Katarzyna Janus is with University of Silesia, Faculty of Computer Science and Materials Science, Institute of Informatics, Department of Biomedical Computer Systems, Będzińska 39, 41-205 Sosnowiec, Poland. (e-mail: kjanus@us.edu.pl).

Sebastian Stach is with University of Silesia, Faculty of Computer Science and Materials Science, Institute of Informatics, Department of Biomedical Computer Systems, Będzińska 39, 41-205 Sosnowiec, Poland. (e-mail: sebastian.stach@us.edu.pl).

the ultrasonic device to remove the oil. Cleaning the substrate helps the adhesion of film to the substrate and also the quality and speed of vacuum. The glass and silicon substrates are placed circularly on the substrate on the electrode attached to the ground within target range. The purpose of this idea is the same distance from the target center and consequently is the same deposition condition. The chamber is vacuumed before the deposition using rotary and diffusion pumps to the pressure of 10^{-5} mbar, and when the chamber pressure is reached the considered pressure with entering acetylene gas, the RF power is applied. Afterward, the nickel layers are fabricated at room temperature according to Table I.

Table I. Conditions used for preparing samples.

ID	Target	Sputtering parameters			Deposition time [min]
		Basic preassure [mbar]	Working preassure [mbar]	Power [W]	
#1	Ni	10^{-5}	0.025	250	7
#2	Ni	10^{-5}	0.025	250	10
#3	Ni	10^{-5}	0.025	250	13

B. Measuring data acquisition

The samples 1, 2 and 3 presented above with detailed determined parameters of sputtering obtained by means of atomic force microscope (AFM), were submitted for analysis by MountainsMap ® Premium program version 6.2.7200 developed by Digital Surf [41]. All images were obtained over square areas of 1 μm x 1 μm.
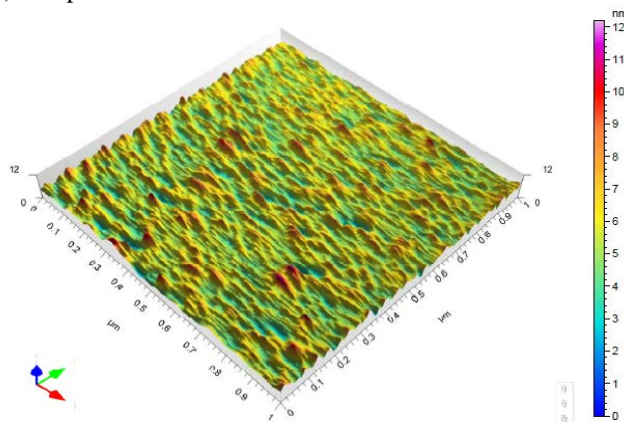
a) Sample 1

Fig. 1. 3-D surface image of sample 1 after the analysis with AFM

MountainsMap software allows creating a height histogram (Fig. 2). It is the height distribution determined by the number of the surface elements corresponding to a certain peak height. The picture below shows also areal material ratio curve, which begins at the highest surface spot (marked as 0%) and has it's end in the lowest surface spot (marked as 100%).
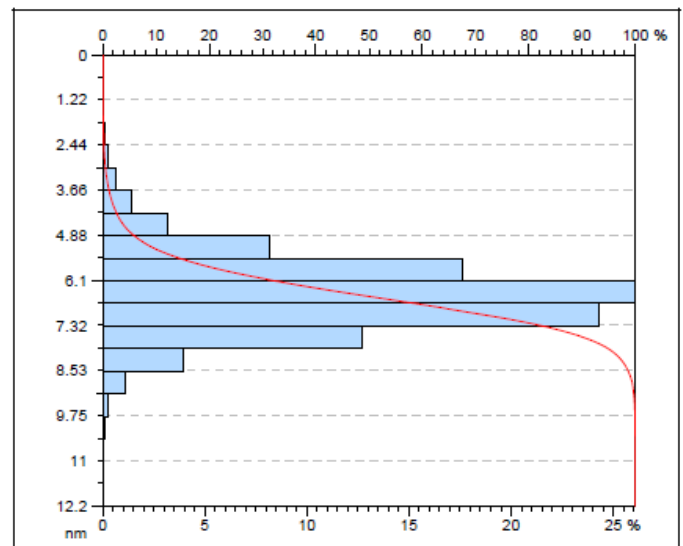

Fig. 2. Height distribution histogram and areal material ratio curve for sample 1

Using areal material ratio curve (marked with red color) a set of parameters was represented: *Sk*, *Svk*, *Spk* as well as *Smr1* and *Smr2* (Fig. 3). *Sk* parameter describes the depth of the core. It is calculated using a linearized line intersecting X axis on 0% and 100%. Using this method, two lines parallel to X axis are constructed. That provides the value of parameter *Sk* = 2.32 nm.

Values of parameters *Smr1* and *Smr2* are calculated using lines parallel to Y axis that are intersecting with lines parallel to X axis, that were used in calculation of parameter *Sk*. *Smr1* parameter is a value of areal material ratio of peaks with value of 11.9%, while *Smr2* stands for value of areal material ratio of dales and reaches the value of 91.1%.

Svk and *Spk* parameters are determined by the height of the perpendicular triangles depicted on the diagram (orange color) and they stand for reduced dale height (*Svk* = 0.974 nm) and reduced peak height (*Spk* = 1.37 nm).

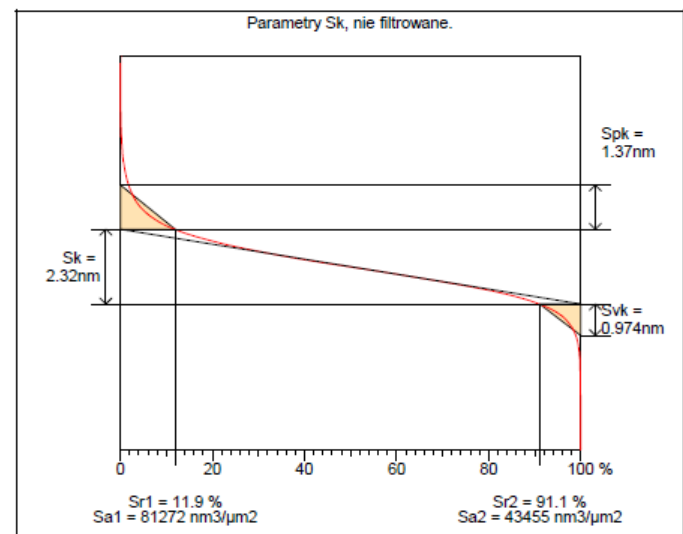Fig. 3. Areal material ratio curve with parameters: Sk, Spk, Svk, Smr1 and Smr2 for the sample 1.

Indicators *Vmp*, *Vmc*, *Vvci*, *Vvv* (Fig. 4) belong to the volume functional parameters group and are calculated analogically to the previous attributes – using information included on the areal material ratio curve. The calculation is executed based on calculated level of parameters *mr1* (10%) and *mr2* (80%).

Peak material volume (*Vmp*) equals to 0.00000709 ml/m^2, which characterizes the volume of analyzed compound for the area filled with material at *mr1* (10%) level. The difference between height of this two indicators *mr2* (80%) and *mr1* (10%) designates core material volume (*Vmc* = 0.000807 ml/m^2). Dale void volume (*Vvv*) equals to 0.000102 ml/m^2 and is related to the area filled with material at *mr2*(80%) level, as well as to the surface deprived of material at *mr1* level. The last indicator, core void volume (*Vvc* = 0.00119 ml/m^2), is inversed *Vmc* parameter, because it is calculated through the difference between *mr1* and *mr2*.

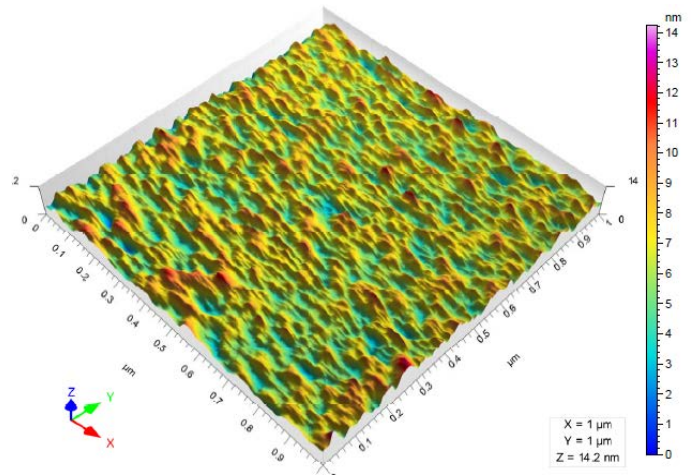

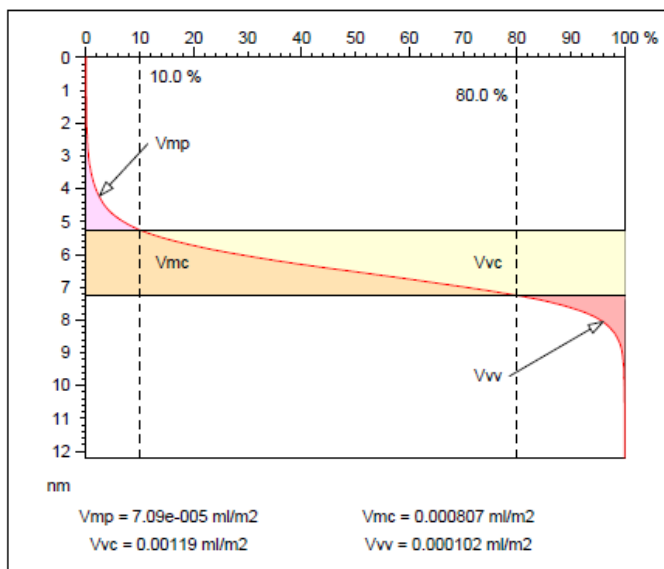Fig. 5. 3-D surface image of sample 2 after the analysis with AFM

Fig. 4. Areal material ratio curve with parameters: Vmp, Vmc, Vvc and Vvv for the sample 1.

In reference with generated images of the sample, all of the functional parameters related to the surface of the analyzed nickel-coal compound were calculated in accordance with ISO 25178 (Table 2) and EUR 15178N norm [42].
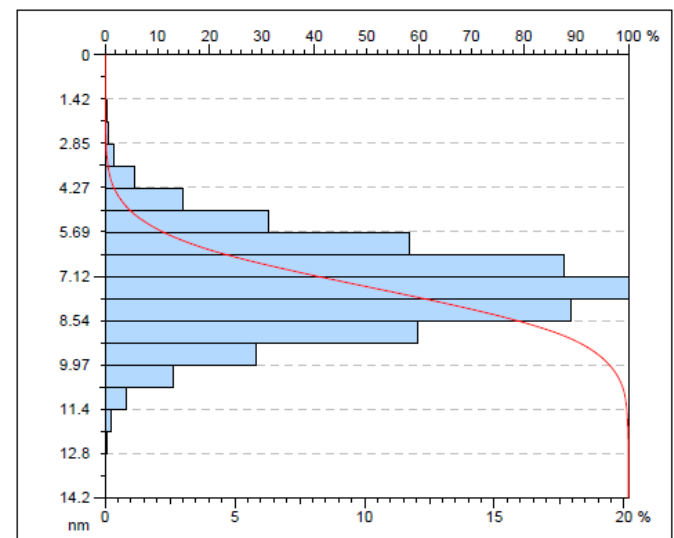
b) Sample 2

For the sample 2 the same operations were carried out in order to receive functional parameter characteristics placed below, e.g. height histogram with areal material ratio curve (Fig. 6).

Fig. 6. Height distribution histogram and areal material ratio curve for sample 2

Areal material ratio curve and parameters *Sk*, *Spk*, *Svk*, *Smr1* and *Smr2* (Fig. 7) for sample 2 were calculated the same way, their values are respectively: *Sk* = 3.63 nm, *Spk* = 1.47 nm, *Svk* = 1.43 nm, *Smr1* = 10.3 %, *Smr2* = 90.7%.
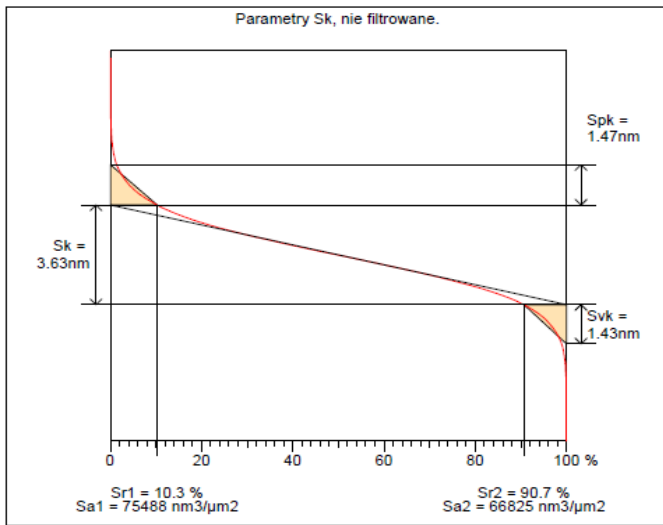
Fig. 7. Areal material ratio curve with parameters: Sk, Spk, Svk, Smr1 and Smr2 for the sample 2.

Volume attributes take values as stated: $Vmp = 0.0000748$ ml/m^2, $Vmc = 0.00$ ml/m^2, $Vvc = 0.00174$ ml/m^2 and $Vvv = 0.000158$ ml/m^2 (Fig. 8).
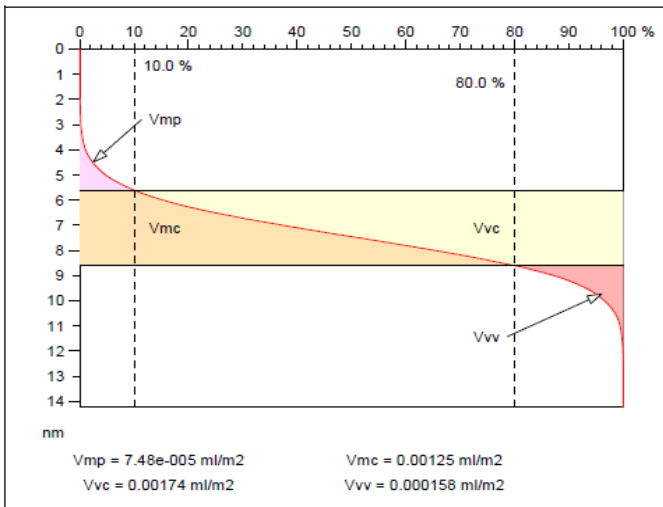

Fig. 8. Areal material ratio curve with parameters: Vmp, Vmc, Vvc and Vvv for the sample 2.

c) Sample 3

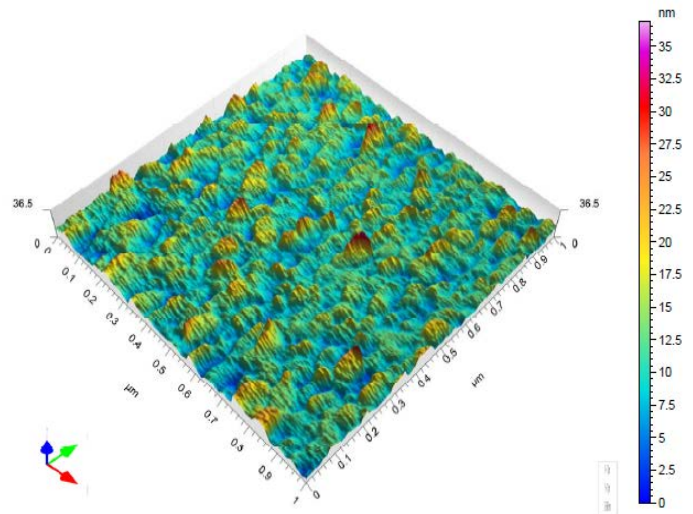Fig. 9. 3-D surface image of sample 3 after the analysis with AFM

Analyzed nickel-coal compound of sample 3 was examined in the same way as previous samples (Fig. 10).
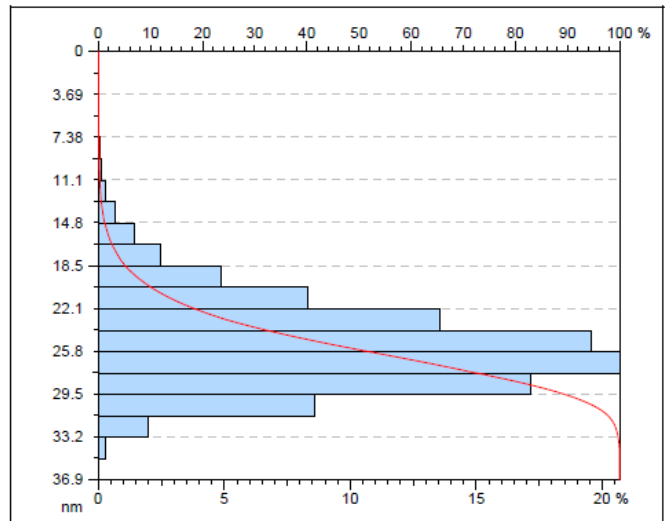

Fig. 10. Height distribution histogram and areal material ratio curve for sample 3

Parameters *Sk*, *Spk*, *Svk*, *Smr1*, *Smr2* have next values: *Sk* = 9.00 nm, *Spk* = 5.39 nm, *Svk* = 2.19 nm, *Smr1* = 13.4 %, *Smr2* = 93.4 % (Fig. 11).
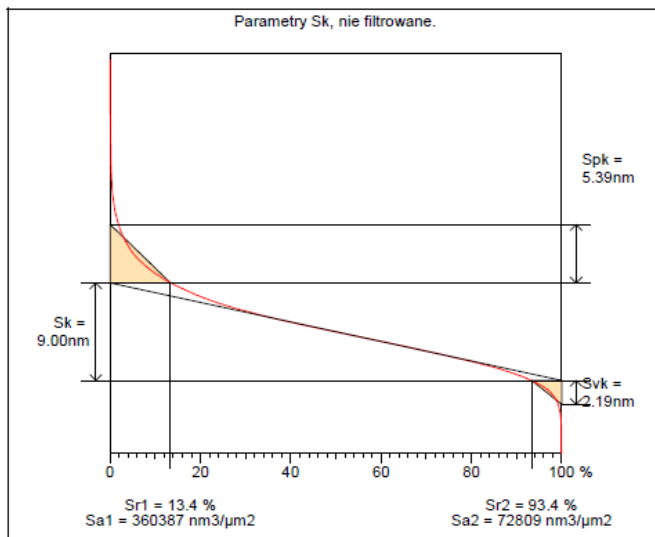
Fig. 11. Areal material ratio curve with parameters: Sk, Spk, Svk, Smr1 and Smr2 for the sample 3.

The volume factors Vmp, Vmc, Vvc, Vvv which have values of: $Vmp = 0.000264$ ml/m^2, $Vmc = 0,00317$ ml/m^2, $Vvc = 0,00496$ ml/m^2, $Vvv = 0,00296$ ml/m^2 (Fig. 12).
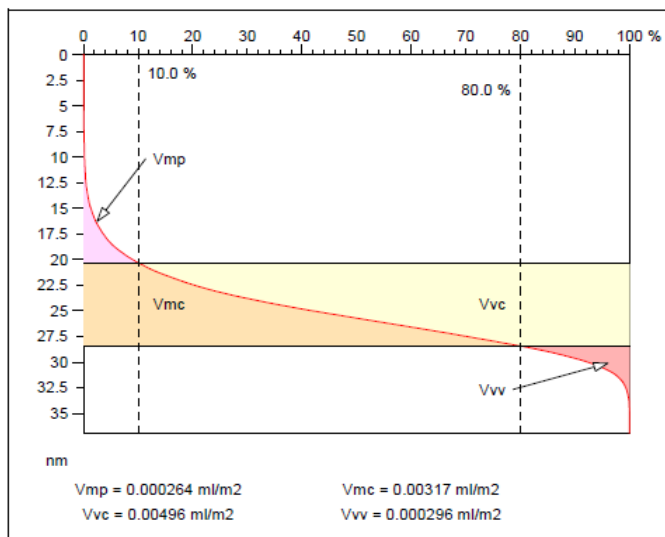

Fig. 12. Areal material ratio curve with parameters: Vmp, Vmc, Vvc and Vvv for the sample 3.

Table II. The values of 3-D functional parameters for samples 1, 2 and 3 in accordance with ISO 25178 norm.

ISO 25178			
Parameter	Sample 1	Sample 2	Sample 3
Smr [%]	100	100	100
Smc [nm]	1.22	1.83	4.99
Sxp [nm]	1.75	2.76	5.57
Vm [µm^3/µm^2]	0.0000709	0.0000748	0.000264
Vv [µm^3/µm^2]	0.00129	0.0019	0.00525
Vmp [µm^3/µm^2]	0.0000709	0.0000748	0.000264
Vmc [µm^3/µm^2]	0.000807	0.00125	0.00317
Vvc [µm^3/µm^2]	0.00119	0.00174	0.00496
Vvv [µm^3/µm^2]	0.000102	0.000158	0.000296

III. ANALYSIS OF RESULTS

In addition, during the examination of nickel-coal compound, three diagrams were drawn for each sample. First diagram is a height histogram illustrated by the amount of elements appearing on the surface related to a certain peak height along with areal material curve, which is superimposed on the histogram. Second diagram represents areal material curve with parameter values of: Sk, Svk, Spk, $Smr1$ and $Smr2$, which are marked on the diagram the way they were calculated from the diagram. Third diagram is a visualization and calculation of volume parameters: Vmp, Vmc, Vvc and Vvv using areal material curve.

Parameters belonging to the group of functional parameters have various values. Areal material ratio Smr, possessing a certain height in spot c is the same for all the samples and equals to 100%. The value of inverse areal material ratio Smc is the lowest for sample number 1 and equals to 1.22 nm, when the highest value was recorder for sample number 3 with value of 4.99 nm. That presents the height of cross section of spot c. Peak extreme height has the highest value for sample number 3 (5.57 nm), and the lowest for sample number 1 (1.75 nm).

By analyzing areal material ratio curve, which encloses spots: Sk, Svk, Spk, $Smr1$ and $Smr2$ it was observed, that core roughness height Sk calculated as a difference between two extreme levels (maximal and minimal) of surface core, reaches the highest value for sample number 3 (9.00 nm) and the lowest for sample number 1 (2.32 nm). Parameters Svk and Spk stand for reduced dale height and reduced peak height and for both of these, the highest value were recorded for sample number 3 ($Svk = 2.19$ nm; $Spk = 5.39$ nm) and the lowest for sample number 1 ($Svk = 0.974$ nm; $Spk = 1.37$ nm). Factors $Smr1$ and $Smr2$ in contrast to the other parameters reach the highest values for sample number 3 ($Smr1 = 13.4\%$; $Smr2 = 93.4\%$) but the lowest for sample number 2 ($Smr1 = 10,3\%$; $Smr2 = 90,7\%$).

Group of volume functional parameters include factor Vv, that stands for void volume and it reaches the highest value for sample number 3 (0.00525 µm^3/µm^2) and the lowest value for sample number 1 (0.00129 µm^3/µm^2).

The smallest material volume was recorded for sample number 1 (0.0000709 µm^3/µm^2), the highest for sample number 3 (0.000264 µm^3/µm^2) and it is indicated by Vm factor. Peak material volume Vmp has the highest value for sample number 3 (0.000264 µm^3/µm^2), minimal for sample number 1 (0.0000709 µm^3/µm^2).

Parameter Vmc describing core material volume assumes the lowest value for sample number 1 (0.000807 µm^3/µm^2), and the highest for sample number 3 (0.00317 µm^3/µm^2). The difference in void volume between material indicators $mr1$ and $mr2$, which is Vvc parameter that reaches minimum for sample

number 1 (0.00119 $\mu m^3/\mu m^2$), and maximum for sample number 3 (0.00496 $\mu m^3/\mu m^2$). The last of volume parameters – *Vvv* standing for dale void volume of cavity in surface of the area deprived of material, has the lowest value recorded for sample number 1 (0.000102 $\mu m^3/\mu m^2$) and the highest for sample number 3 (0.000296 $\mu m^3/\mu m^2$).

IV. CONCLUSION

The quantitative parameters that characterize the surface micromorphology of the nickel–carbon nanocomposite thin films composed of Ni nanoparticles with different average sizes embedded in amorphous hydrogenated carbon, prepared by RF-PECVD were calculated and used to demonstrate the difference between the three samples of different sedimentation time (7, 10, and 13 minutes). It could be concluded that the results with texture characteristics could be used in graphical models for automatic texturing simulation.

APPENDIX

The statistical parameters of 3D surface roughness, according with ISO 25178-2: 2012 are defined as follows [42-47]:

a) Height parameters are a class of surface finish parameters that quantify the Z-axis perpendicular to the surface.

(Sq) – Root mean square height is the standard deviation of the height distribution, or RMS surface roughness.

(Ssk) – Skewness is the third statistical moment, qualifying the symmetry of the height distribution. Negative skew indicates a predominance of valleys, while positive skew is seen on surfaces with peaks.

(Sku) – Kurtosis is the fourth statistical moment, qualifying the flatness of the height distribution. For spiky surfaces, Sku > 3; for bumpy surfaces, Sku < 3; perfectly random surfaces have kurtosis of 3.

(Sp) - Maximum peak height is the height between the highest peak and the mean plane.

(Sv) - Maximum pit height is the depth between the mean plane and the deepest valley.

(Sz) - Maximum height is the height between the highest peak and the deepest valley.

(Sa) - Arithmetical mean height is the mean surface roughness.

b) Functional parameters are calculated from the Abbott-Firestone curve obtained by the integration of height distribution on the whole surface.

(Smr) - Areal material ratio is the bearing area ratio at a given height. Ratio of the area of the material at a specified height c (cut level) to the evaluation area. The Smr(c) is expressed as a percentage. For the Smr parameter, the height c is counted by default from the mean plane. In our study, c = 1 μm under the highest peak.

(Smc) - Inverse areal material ratio is the height c at which a given areal material ratio p is satisfied. The height is calculated from the mean plane. In our study, p = 10%.

(Sxp) - Extreme peak height is the difference in height between q% and p% material ratio. This parameter must be configured with two thresholds entered in %. In our study, p = 50%, q = 97.5%.

c) Spatial parameters describe topographic characteristics based upon spectral analysis. They quantify the lateral information present on the X- and Y-axes of the surface.

(Sal) - Auto-correlation length is the horizontal distance of the autocorrelation function (tx, ty) which has the fastest decay to a specified value s, with 0 < s < 1. The default value for s in the software is 0.2. This parameter expresses the content in wavelength of the surface. A high value indicates that the surface has mainly high wavelengths (low frequencies). In our study, s = 0.2.

(Str) - Texture-aspect ratio is the ratio of the shortest decrease length at 0.2 from the autocorrelation, on the greatest length. This parameter has a result between 0 and 1. If the value is near 1, we can say that the surface is isotropic, i.e. has the same characteristics in all directions. If the value is near 0, the surface is anisotropic, i.e. has an oriented and/or periodical structure. In our study, s = 0.2.

(Std) - Texture direction calculates the main angle for the texture of the surface, given by the maximum of the polar spectrum. This parameter has a meaning if Str is lower than 0.5. In our study, Reference Angle = 0°.

d) Hybrid parameters are a class of surface finish parameters that quantify the information present on the X-, Y- and Z-axes of the surface, i.e. those criteria that depend both on the amplitude and the spacing, such as slopes, curvatures etc.

(Sdq) - Root mean square gradient is the root-mean-square slope of the surface.

(Sdr) - Developed interfacial area ratio is the ratio of the increment of the interfacial area of the scale limited surface within the definition area over the definition area. The developed surface indicates the complexity of the surface thanks to the comparison of the curvilinear surface and the support surface. A completely flat surface will have a Sdr near 0%. A complex surface will have a Sdr of some percents.

e) Functional volume parameters are typically used in tribological studies. They are calculated using the Abbott-Firestone curve (areal material ratio curve) calculated on the surface.

Vm(p) - Material volume is the volume of the material at a material ratio p (in %). In our study, p = 10%.

Vv(p) - Void volume is the volume of the voids at a material ratio p (in %). In our study, p = 10%.

Vmp - Peak material volume of the scale limited surface is the volume of material in the peaks, between 0% material ratio and a material ratio p (in %), calculated in the zone above c1. Vmp = Vm(p). In our study, p = 10%.

Vmc - Core material volume of the scale limited surface is the volume of material in the core or kernel, between two material ratios p and q (in %), calculated in the zone between c1 and c2. Vmc = Vm(q) - Vm(p). In our study, p = 10%, q = 80%.

Vvc - Core void volume of the scale limited surface is the volume of void in the core or kernel, between two material ratios p and q (in %), calculated in the zone between c1 and c2. Vvc = Vv(p) - Vv(q). In our study, p = 10%, q = 80%.

Vvv - Pit void volume of the scale limited surface is the volume of void in the valleys, between a material ratio p (in %) and 100% material ratio, calculated in the zone below c2. Vvv = Vv(p). In our study, p = 80%.

REFERENCES

[1] Y. Lei, and W.K. Chim, "Highly Ordered Arrays of Metal/Semiconductor Core–Shell Nanoparticles with Tunable Nanostructures and Photoluminescence," *J. Am. Chem. Soc.*, vol. 127, no. 5, pp. 1487–1492, 2005. DOI: 10.1021/ja043969m.

[2] Ş. Ţălu, C. Luna, A. Ahmadpourian, A. Achour, A. Arman, S. Naderi, N. Ghobadi, S. Stach, and B. Safibonab, "Micromorphology and fractal analysis of nickel–carbon composite thin films," *J. Mater. Sci. Mater. Electron*, vol. 27, no. 11, pp. 11425–11431, 2016. DOI: 10.1007/s10854-016-5268-9.

[3] S. Stach, Ż. Garczyk, Ş. Ţălu, S. Solaymani, A. Ghaderi, R. Moradian, N.B. Nezafat, S.M. Elahi, and H. Gholamali, "Stereometric Parameters of the Cu/Fe NPs Thin Films," *J. Phys. Chem. C*, vol. 119, no. 31, pp. 17887-17898, 2015. DOI: 10.1021/acs.jpcc.5b04676.

[4] M. Molamohammadi, C. Luna, A. Arman, S. Solaymani, A. Boochani, A. Ahmadpourian, and A. Shafiekhani, "Preparation and magnetoresistance behavior of nickel nanoparticles embedded in hydrogenated carbon film," *J. Mater. Sci. Mater. Electron*, vol. 26, no. 9, pp. 6814–6818, 2015. DOI: 10.1007/s10854-015-3294-7.

[5] Ş. Ţălu, *Micro and nanoscale characterization of three dimensional surfaces. Basics and applications*, Cluj-Napoca, Romania: Napoca Star Publishing House, 2015.

[6] S. Stach, W. Sapota, Ş. Ţălu, A. Ahmadpourian, C., Luna, N. Ghobadi, A. Arman, and M. Ganji, "3-D surface stereometry studies of sputtered TiN thin films obtained at different substrate temperatures," *J. Mater. Sci. Mater. Electron*, vol. 28, no. 2, pp. 2113–2122, 2016.

[7] Ş. Ţălu, S. Stach, A. Méndez, G. Trejo, and M. Ţălu, "Multifractal characterization of nanostructure surfaces of electrodeposited Ni-P coatings," *J Electrochem Soc.*, vol. 161, pp. D44-D47, 2014.

[8] S. Ramazanov, Ş. Ţălu, D. Sobola, S. Stach, and G. Ramazanov, "Epitaxy of silicon carbide on silicon: Micromorphological analysis of growth surface evolution. Superlattices and Microstructures," vol. 86, pp. 395-402, 2015. DOI: 10.1016/j.spmi.2015.08.007.

[9] A. Arman, Ş. Ţălu, C. Luna, A. Ahmadpourian, M. Naseri, and M. Molamohammadi, "Micromorphology characterization of copper thin films by AFM and fractal analysis," *J. Mater. Sci. - Mater. Electron.*, vol. 26, no. 12, pp. 9630-9639, 2015.

[10] S. Stach, D. Dallaeva, Ş. Ţălu, P. Kaspar, P. Tománek, S. Giovanzana, and L. Grmela, "Morphological features in aluminum nitride epilayers prepared by magnetron sputtering," *Mater. Sci. Poland*, vol. 33, no. 1, pp. 175-184, 2015.

[11] Ş. Ţălu, S. Stach, D. Raoufi, and F. Hosseinpanahi, "Film thickness efect on fractality of tin-doped In$_2$O$_3$ thin films," *Electronic Materials Letters*, vol. 11, no. 5, pp. 749-757, 2015. DOI: 10.1007/s13391-015-4280-1.

[12] Ş. Ţălu, S. Stach, S. Valedbagi, S.M. Elahi, and R. Bavadi, "Surface morphology of titanium nitride thin films synthesised by DC reactive magnetron sputtering," *Mater. Sci. Poland*, vol. 33, no. 1, pp. 137-143, 2015. DOI: 10.1515/msp-2015-0010.

[13] Ş. Ţălu, A.J. Ghazai, S. Stach, A. Hassan, Z. Hassan, and M. Ţălu, "Characterization of surface roughness of Pt Schottky contacts on quaternary n-Al$_{0.08}$In$_{0.08}$Ga$_{0.84}$N thin film assessed by atomic force microscopy and fractal analysis," *J. Mater. Sci. Mater. El.*, vol. 25, no. 1, pp. 466–477, 2014. DOI: 10.1007/s10854-013-1611-6.

[14] N. Ghobadi, M. Ganji, C. Luna, A. Arman, and A. Ahmadpourian, "Effects of substrate temperature on the properties of sputtered TiN thin films," *J. Mater. Sci. Mater. Electron*, vol. 27, no. 3, pp. 2800–2808, 2016. DOI: 10.1007/s10854-015-4093-x.

[15] Ş. Ţălu, S. Stach, S. Solaymani, R. Moradian, A. Ghaderi, M.R. Hantehzadeh, S.M. Elahi, Ż. Garczyk, and S. Izadyar, "Multifractal Spectra of Atomic Force Microscope Images of Cu/Fe Nanoparticles Based Films Thickness," *J Electroanal. Chem.*, vol. 749, pp. 31-41, 2015. DOI: 10.1016/j.jelechem.2015.04.009.

[16] D. Dallaeva, Ş. Ţălu, S. Stach, P. Škarvada, P. Tománek, and L. Grmela, "AFM imaging and fractal analysis of surface roughness of AlN epilayers on sapphire substrates," *Appl. Surf. Sci.*, vol. 312, pp. 81-86, 2014. DOI: 10.1016/ j.apsusc.2014.05.086.

[17] A. Ahmadpourian, C. Luna, A. Boochani, A. Arman, A. Achour, S. Rezaee, and S. Naderi, "The effects of deposition time on surface morphology, structural, electrical and optical properties of sputtered Ag-Cu thin films," *The European Physical Journal Plus*, vol. 131, no. 10, pp. 381, 2016. DOI: 10.1140/epjp/i2016-16381-2.

[18] T. Ghodselahi, and A. Arman, "Magnetoresistance of Cu–Ni nanoparticles in hydrogenated amorphous carbon thin films," *J. Mater. Sci. Mater. Electron*, vol. 26, no. 6, pp. 4193–4197, 2015. DOI: 10.1007/s10854-015-2965-8

[19] A. Arman, C. Luna, M. Mardani, F. Hafezi, A. Achour, and A. Ahmadpourian, "Magnetoresistance of nanocomposite copper/carbon thin films," *J. Mater. Sci. Mater. Electron*, vol. 28, no. 6, pp. 4713–4718, 2017.

[20] N. Ghobadi, M. Ganji, C. Luna, A. Ahmadpourian, and A. Arman, "The effects of DC power on the physical properties and surface topography of sputtered TiN nanostructured thin films," *Optical and Quantum Electronics*, vol. 48, no. 10, pp. 467, 2016. DOI: 10.1007/s11082-016-0742-4.

[21] V. Dalouji, S. M. Elahi, and S. Naderi, "Surface plasmon resonance and electrical properties of RF: magnetron sputtered carbon–nickel composite films at different annealing temperatures," Rare Metals, vol. 35, no. 11, pp. 863-869, 2016. DOI: 10.1007/s12598-015-0581-7.

[22] S. Naderi, A. Ghaderi, S. Solaymani, and M.M. Golzan, "Structural, optical and thermal properties of silver colloidal nanoparticles," *The European Physical Journal Applied Physics*, vol. 58, no. 2, pp. 20401, 2012. DOI: 10.1051/epjap/2012110310.

[23] X. Gao, X. Zhang, C. Wan, J. Wang, X. Tan, and D. Zeng, "Temperature-dependent resistive switching of amorphous carbon/silicon heterojunctions," *Diamond and Related Materials*, vol. 22, pp. 37-41, 2012. DOI: 10.1016/j.diamond.2011.12.012.

[24] R. Hauert, "A review of modified DLC coatings for biological applications," *Diamond and related materials*, vol. 12, no. 3, pp. 583-589, 2003. DOI: 10.1016/S0925-9635(03)00081-5.

[25] R. Hauert, "An overview on the tribological behavior of diamond-like carbon in technical and medical applications," *Tribology International*, vol. 37, no. 11, pp. 991-1003, 2004. DOI: 10.1016/j.triboint.2004.07.017.

[26] F.Z. Cui, and D.J. Li, "A review of investigations on biocompatibility of diamond-like carbon and carbon nitride films," *Surface and Coatings Technology*. vol. 131, pp. 481-487, 2000. DOI: 10.1016/S0257-8972(00)00809-4.

[27] A. Matthews, and S.S. Eskildsen, "Engineering applications for diamond-like carbon," *Diamond and Related Materials*, vol. 3, no. 4-6, pp. 902-911, 1994. DOI: 10.1016/0925-9635(94)90297-6.

[28] S. V. Hainsworth, V. Sarah, and N. J. Uhure, "Diamond like carbon coatings for tribology: production techniques, characterisation methods and applications," *International materials reviews*, vol. 52, no. 3, pp. 153-174, 2007. DOI: 10.1179/174328007X160272.

[29] A. Erdemir, and C Donnet, "Tribology of diamond-like carbon films: recent progress and future prospects," *Journal of Physics D: Applied Physics*, vol. 39, no. 18, R311, 2006. DOI: 10.1088/0022-3727/39/18/R01.

[30] J.K. Luo, Y.Q. Fu, H.R. Le, J.A. Williams, S.M. Spearing, and W.I. Milne, "Diamond and diamond-like carbon MEMS," *Journal of Micromechanics and Microengineering*, vol. 17, no. 7, pp. S147, 2007. DOI: 10.1088/0960-1317/17/7/S12.

[31] S. Abdolghaderi, B. Astinchap, and A. Shafiekhani, "Electrical percolation threshold in Ag–DLC nanocomposite films prepared by RF-sputtering and RF-PECVD in acetylene plasma," *J. Mater. Sci. Mater. Electron*, vol. 27, no. 7, pp. 6713–6720, 2016. DOI: 10.1007/s10854-016-4620-4.

[32] M.A. Vesaghi, and A. Shafiekhani, "Diamond-like carbon film from liquid gas on metallic substrates," *J. Phys. D: Appl. Phys.*, vol. 32, pp. L101, 1999. DOI: 10.1088/0022-3727/31/12/002.

[33] F. Mashayekhi, A. Shafiekhani, and S.A. Sebt, "Iron nanoparticles embedded in carbon films: structural and optical properties," *Eur. Phys. J. Appl. Phys.*, vol. 74, pp. 30402, 2016. DOI: 10.1051/epjap/2016150508

[34] S.H. Jeong, B.S. Kim, B.T. Lee, J.K. Kim, and H.R. Park, "Structural and optical properties of TiO2 films prepared using reactive RF magnetron sputtering," *J. Korean Phys. Soc.*, vol. 41, no. 1, pp. 67-72, 2002. Reference Number 35028993.

[35] N. Bouts, M. Gaillard, L. Donero, A.A. El Mel, E. Gautron, B. Angleraud, C. Boulmer-Leborgne, and P.Y. Tessier, "Growth control of carbon nanotubes using nanocomposite nickel/carbon thin films," *Thin Solid Films*, vol. 630, pp. 38–47, 2017. DOI: 10.1016/j.tsf.2016.10.025.

[36] B. Bayatsarmadi, Y. Zheng, V. Russo, L. Ge, C. S. S. Casari and S. Qiao "Highly active nickel–cobalt/nanocarbon thin films as efficient water splitting electrodes," *Nanoscale*, vol. 8, no. 43, pp. 18507-18515, 2016. DOI: 10.1039/C6NR06961D.

[37] M. Molamohammadi, A. Arman, A. Achour, B. Astinchap, A. Ahmadpourian, A. Boochani, S. Naderi, and A. Ahmadpourian, "Microstructure and optical properties of cobalt–carbon nanocomposites prepared by RF-sputtering," *J. Mater. Sci. Mater. Electron*, vol. 26, no. 8, pp. 5964-5969, 2015.

[38] A. Arman, T. Ghodselahi, M. Molamohammadi, S. Solaymani, H. Zahrabi, and A. Ahmadpourian, "Microstructure and Optical Properties of Cu@Ni Nanoparticles Embedded in aC:H," *Prot. Met. Phy. Chem*, vol. 51, no. 4, pp. 575–578, 2015.

[39] S.M. Cherif, A. Layadi, J. Ben Youssef, C. Nacereddine, and Y. Roussigne, "Study of the magnetic anisotropy in Ni/Cu and Ni/glass thin films," *Physica B*, vol. 387, no. 1-2, pp. 281-286, 2007. DOI: 10.1016/j.physb.2006.04.037.

[40] Harish C. Barshilia, and K.S. Rajam, "Characterization of Cu/Ni multilayer coatings by nanoindentation and atomic force microscopy," *Surface and Coatings Technology*, vol. 155, pp. 195-202, 2002. DOI: 10.1016/S0257-8972(02)00008-7.

[41] MountainsMap® 7 Software (Digital Surf, Besançon, France). Available from: http://www.digitalsurf.fr (last accessed June 10th, 2017).

[42] ISO 25178-2: 2012 Geometrical product specifications (GPS) – Surface texture: Areal – Part 2: Terms, definitions and surface texture parameters. (2012) http://www.iso.org. Last accessed October 10th, 2017.

[43] Ş. Ţălu, "Characterization of surface roughness of unworn hydrogel contact lenses at a nanometric scale using methods of modern metrology," Polym. Eng. Sci., vol. 53(10), pp. 2141–2150, 2013.

[44] Ş. Ţălu, and S. Stach, "Multifractal characterization of unworn hydrogel contact lens surfaces," Polym. Eng. Sci., vol. 54(5), pp. 1066–1080, 2014.

[45] Ş. Ţălu, S. Stach, J. Zaharieva, M. Milanova, D. Todorovsky, and S. Giovanzana, "Surface roughness characterization of poly(methyl-methacrylate) films with immobilized Eu(III) β-Diketonates by fractal analysis," Int. J. Polym. Anal. Charact., vol. 19(5), pp. 404-421, 2014.

[46] Ş. Ţălu, S. Stach, A. Mahajan, D. Pathak, T. Wagner, A. Kumar, and R.K. Bedi, "Multifractal analysis of drop-casted copper (II) tetrasulfophthalocyanine film surfaces on the indium tin oxide substrates," Surf. Interface Anal., vol 46(6), pp. 393–398, 2014.

[47] D. Elenkova, J. Zaharieva, M. Getsova, I. Manolov, M. Milanova, S. Stach, and Ş. Ţălu, "Morphology and Optical Properties of SiO₂-Based Composite Thin Films with Immobilized Terbium(III) Complex with a Biscoumarin Derivative," Int. J. Polym. Anal. Charact., vol. 20(1), pp. 42-56, 2015.

Ştefan Ţălu was born in Floreşti, Vaslui county, Romania, on July 31, 1964. He graduated as a mechanical engineer from University of Craiova, Faculty of Mechanics, Romania in 1988. He received his Ph.D. degree (in technical sciences with specialty in technology of machine building) and Associate Professor from the Technical University of Cluj-Napoca, Cluj county, Romania, in 1998 and 2002 respectively.

He is in an academic position in The Technical University of Cluj-Napoca, The Directorate of Research, Development and Innovation Management (DMCDI), Constantin Daicoviciu Street, no. 15, Cluj-Napoca, 400020, Cluj county, Romania, http://research.utcluj.ro.

He has published 19 books, 1 chapter in book in English and 327 scientific papers (180 papers as single author or first author), in journals, at symposia and scientific national and international conferences, in country or abroad. Among them: 71 papers in ISI quoted journals, 140 papers in international databases, 36 papers at national conference and 80 papers at international conferences, published in collaboration with 250 researchers from 21 countries: Italy, USA, UK, Poland, Mexico, Iraq, Malaysia, Serbia, India, Czech Republic, Bulgaria, Iran, Russian Federation, Croatia, Slovakia, Turkey, Hungary, Spain, Canada, China and Colombia.

He currently cooperates with 21 research centres from abroad. He has a number of 300 public presentations at national and international scientific events. He was a member of the research team, during 2001 - 2016, at: 7 national research projects and 2 international research projects. He was Project Manager at: two national research projects and at 7 national research projects with Romanian economic partners.

He was in abroad as: General chair of International scientific events (5); Honor-chair of International scientific events (1); and Editor of International scientific events (1); Member of the Technical Program Committee of International scientific events (79). He has 5 themes/research grants: - new products and original technologies. He has 30 awards from the UEFISCDI, Romania, http://uefiscdi.gov.ro. He is member of 8 journals as editorial board member and of 34 journals as scientific reviewer.

Currently he is a member of The International Society of the Arts, Mathematics and Architecture (ISAMA); The International Association of Engineers (IAENG); International Association of Advanced Materials (IAAM), Sweden; Athens Institute for Education and Research (ATINER), Athens, Greece, and of The Romanian Committee for History and Science Philosophy and Technics (CRIFST) of Cluj Branch of Romanian Academy.

Katarzyna Janus was born on 12.02.1994 in Miechów, Poland. On 13.02.2017 she graduated from the first degree studies in biomedical engineering at the University of Silesia, receiving the title of Engineer of Biomedical Engineering.

In the academic year 2016-2017, in the summer semester, she started the second cycle of biomedical engineering and additionally started the second level of medical physics at her mother's university.

In addition, from 2015-2016, she is attending the RCKU Medical School in the direction of technician electroradiologist.

In the academic year 2016-2017 she received the Rector's Scholarship for the best students.

Sebastian Stach was born in Sosnowiec, Poland, on April 10, 1974. In 1999 he graduated from the Faculty of Technology of the University of Silesia in Katowice, and in 2005 he completed his doctoral studies at the Faculty of Mathematics, Physics and Chemistry of the same university, obtaining a PhD degree in technical sciences in the discipline of material engineering.

His habilitation procedure was carried out in 2017 at the Institute of Biocybernetics and Biomedical Engineering of the Polish Academy of Sciences, and resulted in awarding habilitation in technical disciplines in the field of biocybernetics and biomedical engineering.

Since 2000 he has worked as a researcher and lecturer at the Faculty of Computer Science and Materials Science of the University of Silesia in Katowice. He currently works at the Institute of Computer Science in the Department of Computer Biomedical Systems.

His research interests include the following specializations: biomedical engineering, image analysis and processing, biomedical informatics, confocal

microscopy and AFM surface microscopy, quantitative analysis and material surface modelling, material strength.

He has published more than 50 international papers and participated in national and international scientific conferences. He currently cooperates with more than 45 research centres around the world.